Article

Postsynthetic Oxidation of Coordination Site in a Heterometallic Metal-Organic Framework: Tuning Catalytic Behaviors

Yi Han, Michael A. Sinnwell, Robert G. Surbella III, Wenjuan Xue, Hongliang Huang, Jian Zheng, Bo Peng, Gaurav Verma, Yang Yang, Lili Liu, Shengqian Ma, and Praveen K. Thallapally

Chem. Mater., **Just Accepted Manuscript** • DOI: 10.1021/acs.chemmater.0c01267 • Publication Date (Web): 20 May 2020

Postsynthetic Oxidation of Coordination Site in a Heterometallic Metal-Organic Framework: Tuning Catalytic Behaviors

Yi Han,*,† Michael A. Sinnwell,‡ Robert G. Surbella III,‡ Wenjuan Xue,§ Hongliang Huang,§ Jian Zheng,‡ Bo Peng,‡ Gaurav Verma,# Yang Yang,‡ Lili Liu,‡ Shengqian Ma,# Praveen K. Thallapally*,‡

† Key Laboratory of Eco-chemical Engineering, College of Chemistry and Molecular Engineering, Qingdao University of Science and Technology, Qingdao, Shandong 266042, P. R. China.

‡ Pacific Northwest National Laboratory, Richland, WA 99352, United States.

§ State Key Laboratory of Separation Membranes and Membrane Processes, Tianjin Polytechnic University, Tianjin 300387, P. R. China.

Department of Chemistry, University of South Florida, Tampa, Florida 33620, United States.

ABSTRACT: Postsynthetic modification (PSM) in metal-organic frameworks (MOFs) can introduce multiple functionalities and alter the structural function for the desired application. However, the PSM of the coordination site faces the challenges of structural collapse or incompatibility between the original metal site and the newly formed coordination group. Herein, we developed a novel concept of introducing "primary" and "secondary" nodes, coexisting in a water-stable, Zr-based heterometallic MOF, $[Zr_6(\mu_3\text{-}OH)_8(OH)_8][Cu^I_4(L_1)_4]_2$ (**1-SH-a**, H_2L_1 = 6-mercaptopyridine-3-carboxylic acid). The post-synthetic oxidation at the coordination site was successfully achieved in the "secondary" nodes $[Cu^I_4(L_1)_4]^{4-}$, while the robust "primary" nodes $[Zr_6(\mu_3\text{-}OH)_8(OH)_8]^{8+}$ stabilized the whole framework to form $[Zr_6(\mu_3\text{-}OH)_8(OH)_8][(Cu^I_{0.44}Cu^{II}_{0.56}(OH)_{0.56})_4(L_2)_4]_2$ (**1-SO$_3$H**, H_2L_2 = 6-sulfonicotinic acid). Attempts to directly synthesize **1-SO$_3$H** under the reactions of Zr(IV), Cu(II), and H_2L_2 failed. Furthermore, PSM of **1-SH-a** to form **1-SO$_3$H** was utilized to tune the catalytic behaviors toward the styrene oxide ring-opening reaction to give an improved regioselectivity of primary alcohol (A) of ~99% compared with **1-SH-a** (~71%).

INTRODUCTION

Postsynthetic modification (PSM) of porous materials such as mesoporous silica and porous carbons has been successfully used to control and analyze their organization and functionalization.[1,2] In the past decades, much interest has been focused on tailoring metal-organic frameworks (MOFs) using PSM.[3-4] PSM has been extensively used and has become much sought-after compared to de novo synthesis because PSM offers the ability to: (i) facilitate the introduction of a wide variety of chemical functionalities, (ii) maximize the rejection of undesirable byproducts in unpredictable ways, and (iii) endow functions that are thermally labile, which are thwarted almost in solvothermal conditions. Accordingly, MOFs have been vested with significant multi-functionalities, and thus adapting the modified functions in response to exploration for the associated applications.

PSM of MOFs can be broadly divided into three major divisions: unique reactions in terms of (i) metal or linker exchange,[5-6] (ii) covalent modification,[7] and (iii) oxidation/reduction.[8-10] Most of these modifications are carried out on the organic components of the framework. Specifically, linker exchange in readily accessible isoreticular MOF analogues leads to progressively diverse functionalities and properties.[11-15] By contrast, covalent modification allows for chemically modifying the organic struts to either introduce the functionality or functionalize the inherent reactive tags[16-19] (Scheme 1). On the other hand, PSM on the coordination site has not yet been exploited by the MOF community, possibly due to the structural collapse under the conditions required or incompatibility between the original metal and the newly formed coordination group.

The coordination ability of thiol and sulfonic groups has been popularized by their extensive use in materials science.[20,21] Generally, thiol preferentially coordinates with soft Lewis acids

(*i.e.*, Cu(I), Ag(I), Au(III)), while the sulfonic group shows affinity for the harder ones (*i.e.*, Cu(II), Ni(II), Fe(II)). In addition, the vulnerability of thiol compounds to oxidize to the sulfonate derivatives assisted by H_2O_2 is well documented even in porous supports, such as thiol grafted single-walled carbon nanotubes.[22] The unique use in coordination chemistry and ready conversion toward thiol and sulfonic groups would enable the preparation of a specific thiolated MOF and permit the formation of the isolated sulfonate one employing postsynthetic oxidation.

Scheme 1. Generic schemes for (a) linker exchange, (b) covalent PSM, and (c) coordination site PSM.

Herein, we report a water-stable heterometallic Zr-MOF $[Zr_6(\mu_3\text{-}OH)_8(OH)_8][Cu^I_4(L_1)_4]_2 \cdot x$guest (**1-SH**, H_2L_1 = 6-mercaptopyridine-3-carboxylic acid), which can undergo a guest-dependent structural transformation to form **1-SH-a**. As expected, in the presence of H_2O_2, the coordination site modification was successfully achieved in **1-SH-a** by postsynthetic oxidation of L_1^{2-} to the corresponding L_2^{2-} (H_2L_2 = 6-sulfonicotinic acid) (Scheme 1c). The resulting **1-SO$_3$H** was determined by powder X−ray diffraction (PXRD), X−ray photoelectron spectroscopy (XPS), and nuclear magnetic resonance (^{1}H NMR). Significantly, the styrene oxide ring-opening reactions catalyzed by **1-SH-a** and **1-SO$_3$H** were thoroughly investigated to compare their catalytic behaviors derived from their modified organic fragments and copper species, indicating that the functionalization of **1-SH-a** to form **1-SO$_3$H** tuned the catalytic behavior to give an improved regioselectivity of primary alcohol (A) of ~99% compared with **1-SH-a** (~71%).

Figure 1. Rational design of BUT-52 and **1-SH** on the basis of In(III) or Zr(IV), Cu(I), and the *in-situ* synthesized L_1^{2-}.

EXPERIMETAL SECTION

Unless otherwise noted, all starting materials were directly purchased from commercial suppliers and used without further purification. $ZrCl_4$ (>99.5+%, Alfa Aesar), CuI (99.0%, ARCOS), 6,6’ -Dithiodinicotinic Acid (H_2L) (>98.0%, TCI), 6-Mercaptopyridine-3-carboxylic acid (H_2L_1) (90%, Sigma-Aldrich), Benzoic Acid (>99%, TCI), Hydrogen Peroxide Solution (H_2O_2) (30 wt. % in H_2O, ACS reagent, Sigma-Aldrich), N,N-Dimethylformamide (DMF) (>99.8%, GR ACS), acetonitrile (CH_3CN) (99.8%, Sigma-Aldrich), dichloromethane (CH_2Cl_2), (99.5+%, Alfa Aesar), acetone (99.5%, Fisher) styrene oxide (98+%, Alfa Aesar), isopropanol (99.6%, ARCOS), 1-bromo-3,5-difluorobenzene (98%, Alfa Aesar), tetrahydrofuran (THF) (99.9%, Sigma-Aldrich), methanol (95%, Fisher), ethanol (95%, Fisher). 6-sulfonicotinic acid (H_2L_2) was synthesized according to the reported literature.[23]

Synthesis of 1-SH. A mixture of $ZrCl_4$ (100 mg), CuI (142.5 mg), and H_2L (61.6 mg) in presence of benzoic acid (2 g) dissolved in N,N-dimethylformamide (DMF, 10 mL) and acetonitrile (CH_3CN, 5 mL) in a 20 mL vial was heated at 120 °C for 96 h. Yellow single crystals in 56% yield (based on H_2L) were harvested.

Synthesis of 1-SH-a. As-synthesized single crystals of **1-SH** was thoroughly washed by fresh DMF and then soaking in acetone for 12 h to produce single crystals of **1-SH-a**. Elemental analysis (EA) (%): Calcd for $C_{57}H_{62}Cu_8N_8O_{37}S_8Zr_6$ = $[Zr_6(\mu_3\text{-}OH)_8(OH)_8][Cu^I_4(L_1)_4]_2 \cdot 3(C_3H_6O) \cdot 2H_2O$: C, 24.77; H, 2.26; N, 4.06; S, 9.28; Found: C, 25.01; H, 1.99; N, 4.02; S, 9.32. The resulting molecular formula was derived from the combination of EA and thermogravimetric analysis (TGA). The solid was continued to soaking in acetone for 5 days, during which acetone was decanted and freshly replenished two times, and then dried at 120 °C under vacuum for 12 h to yield activated sample.

Synthesis of 1-SO$_3$H. As-synthesized single crystals of **1-SH-a** (~ 30 mg) were immersed in a mixture of THF (4 mL)/H_2O_2 (0.1 ml) for 12 h, during which THF/H_2O_2 was decanted and freshly replenished two times. The resulting green crystals was washed by THF and dried in air. EA (%): Calcd for $C_{63}H_{74}Cu_8N_8O_{38}S_8Zr_6$ = $[Zr_6(\mu_3\text{-}OH)_8(OH)_8][(Cu^I_{0.44}Cu^{II}_{0.56}(OH)_{0.56})_4(L_2)_4]_2 \cdot 3(C_4H_8O) \cdot (C_3H_6O) \cdot 2H_2O$: C, 26.42; H, 2.60; N, 3.91; S, 8.96; Found: C, 26.22; H, 3.01; N, 3.88; S, 9.10. Inductively coupled plasma atomic emission spectroscopy (ICP-AES) confirmed the ratios of Zr/Cu upon digestion of **1-SO$_3$H** in dilute H_2O/HNO_3, showing the concentrations of Zr and Cu are 49.8 and 49.6 ppm, respectively, corresponding to the molar ratio of Zr/Cu to be ~ 0.7, which is close to the ratio of Zr/Cu (0.75) in **1-SH**. The activated sample was obtained by soaking in acetone for 5 days and dried at room temperature under vacuum for 24 h.

RESULTS AND DISCUSSION

Solvothermal reactions of $ZrCl_4$, CuI, 6,6’ -Dithiodinicotinic (H_2L) and benzoic acid in a mixture of DMF/CH_3CN at 120 ˚C afforded yellow single crystals of **1-SH**. Single-crystal X-ray diffraction (SCXRD) reveals that **1-SH** crystallizes in the tetragonal space group $P4_2/mnm$ and has a three-dimensional flu topology, which consists of the 8-connected $[Zr_6(\mu_3\text{-}OH)_8(OH)_8]^{8+}$ clusters (denoted “primary” nodes) linked by

tetrahedral $[Cu^{I}_4(L_1)_4]^{4-}$ metalloligands (denoted "secondary" nodes). Similar to our previously reported framework BUT-52,[24] both H_2L_1 are originated from the cleavage of S−S bond during the solvothermal reaction and are allowed to form distinct cuprous sulfur cluster-based heterometallic MOFs (Figure 1). Unlike the 6-connected $[Cu^{I}_6(L_1)_6]^{6-}$ moiety observed in BUT-52, in **1-SH**, a 4-connected $[Cu^{I}_4(L_1)_4]^{4-}$ tetrahedra with D_{2d} symmetry is achieved (Figure. S1). Moreover, an open dodecahedral cageis observed with dimensions of about 22.8×22.8×29.3Å^3, which is constructed by six $[Zr_6(\mu_3\text{-}OH)_8(OH)_8]^{8+}$ and eight $[Cu^{I}_4(L_1)_4]^{4-}$ tetrahedra as vertices and twenty-four L_1^{2-} linkers as edges (Figure S2).

Figure 2. Experimental and simulated PXRD patterns of **1-SH** and **1-SH-a**; inset is the structural transformation from **1-SH** to **1-SH-a**.

An interesting feature in the PXRD pattern of dried bulk **1-SH** after acetone washing resulted in the peak shift, compared to the calculated pattern from the single crystal data, inferring a guest-dependent structural transformation (Figure 2). The size and shape of single crystals after acetone treatment remains unaltered indicative of a single-crystal to single-crystal transformation (Figure. S3). This prompted us to obtain the transformed structure (**1-SH-a**) using SCXRD. **1-SH-a** exhibits very similar unit cell parameters (Table S1), but with a shrink angle in the window compared to that of **1-SH** (Figure 2 insert). Significantly, the calculated PXRD pattern matched well with the as-synthesized **1-SH-a**. Unlike the varied flexibility presented by the previously reported Zr-MOFs in response to guest molecules,[25,26] **1-SH** was found to exclusively maintain its contracted conformation upon immersion in different solvents, showing no guest solvent dependence (Figure S4). TGA and PXRD indicated that **1-SH-a** did not decompose until 350°C in air (Figures S4 and S5). Upon acetone exchange and activation at 120°C, **1-SH-a** showed no N_2 uptake at 77 K, which is most likely due to the insufficient activation and pore size selectivity.[27] However, effective CO_2 adsorption at 273 K was measured with maximum capacity of 40.1 cm^3 g^{-1}, which showed type I adsorption isotherm (Figure S6). The chemical stability of **1-SH-a** was measured by soaking in water for 12 h, where the crystallinity and porosity were maintained as evidenced by PXRD and CO_2 adsorption (Figures S5 and S6). These results demonstrate that the high connectivity "primary" (Zr_6) nodes[28] and robust "secondary" Cu_4S_4 nodes (pK_a (Cu_2S) = 47.6)[29] in **1-SH-a** are responsible for the excellent thermal and chemical stability.

Figure 3. XPS spectra in the regions of (a) Cu 2p and (b) S 2p for **1-SH-a** and **1-SO$_3$H**. (c) ^{1}H NMR spectrum of commercially available H_2L_1 (1), as-synthesized H_2L_2 (2) and DCl/D_2O digested **1-SO$_3$H** in DMSO-d_6 solution (3). Note: We found there is trace H_2L_2 in commercially available H_2L_1 from Sigma-Aldrich Co. (purity: 90%).

Due to the combination of exceptional thermal and chemical stability of **1-SH-a** and the nature of vulnerability of thiol compounds to oxidize to the sulfonate derivatives, the exploration for postsynthetic oxidation of coordination site seemed to be very promising. Therefore, as-synthesized **1-SH-a** was treated in a mixed solution of THF/H_2O_2 (v/v = 4/0.1) at room temperature for 12 h to produce **1-SO$_3$H** (Figure S7). XPS data showed the sulfur 2p region of **1-SH-a** showed that the peak centered at ~162.3 eV corresponded to a reduced oxidation state of sulfur as in L_1^{2-}, while in **1-SO$_3$H**, this peak is absent and a new characteristic band at ~167.6 eV formed, which is assigned to a higher oxidation state of sulfur (L_2^{2-}) (Figure. 3a).[30] Similarly, an intense asymmetrical Cu $2p_{3/2}$ photoelectron peak together with shakeup satellite peaks indicated mixed valence state of Cu in green crystals of **1-SO$_3$H** (Figure S7), which can be deconvoluted into two contributions located at 932.1 and 934.6 eV, corresponding to Cu(I) $2p_{3/2}$ and Cu(II) $2p_{3/2}$, respectively. Integration of the Cu(I) $2p_{3/2}$ and Cu(II) $2p_{3/2}$ peaks with Cu(II) satellite peaks gives a calculated ratio of Cu(II)/Cu(I) to be ~ 0.56/0.44 in **1-SO$_3$H**. In **1-SH-a**, a strong characteristic band at 932.1 eV is consistent with Cu(I) $2p_{3/2}$, indicating that the Cu species possess 1+ oxidation state (Figure 3b).[31] Further, ^{1}H NMR upon digestion of **1-SO$_3$H** in dilute DCl/D_2O and DMSO-d_6 solution confirmed the degree of conversion by oxidation. It is obvious that the appearance of pure resonances centered at δ 8.91, 8.21, and 7.73 ppm are shown, corresponding to different hydrogen signals in H_2L_2 (Figure 3c). The conversion from -S$^-$ to -SO_3^- highlights the fact that the oxidation can access both the exterior and the interior of the MOF crystal, contributing to overall modification of the organic linkers. FT-IR spectra also indicated that the characteristic S−O stretches of R-SO_3^- in **1-SO$_3$H** were evident at 1244 and 1201 cm^{-1},[21] which were not absent in **1-SH-a** (Figure S8). Continued oxidation of **1-SO$_3$H** for another 12 h can lead to **1-SO$_3$H-a** with an increased ratio of Cu(II)/Cu(I) being ~0.78/0.22, however, causing partial structural collapse (Figures 3b and S4). Despite the incomplete conversion of Cu(I), the percent sulfonation of **1-SH-a** is 100% during the oxidation, indicating the first example of coordination site modification through PSM in MOF materials. In addition, no obvious reversible process from -SO_3^- to -S$^-$ was observed when soaking **1-SO$_3$H** (~ 30 mg) in a saturated THF/H_2O (2 ml/2 ml) solution of reduced agent, such as $NaNO_2$ for 10 days (Figure S11). Attempts to directly synthesize **1-SO$_3$H** under the reactions of Zr(IV), Cu(I)/Cu(II), and pure H_2L_2, however, failed. Furthermore, BUT-52 was also investigated under the same condition for this modification. The PXRD patterns indicated that

the material lost crystallinity, albeit the color change from red to green was observed (Figure S4 and S7). Clearly, the access of robust "primary" nodes seems extremely critical for stabilization of the whole framework, while postsynthetic oxidation can occur in "secondary" nodes.

Figure 4. (a) PXRD patterns of simulated or as-synthesized **1-SH**, **1-SH-a**, and **1-SO_3H**. (b) DFT optimized structure of **1-SO_3H**. (Only the optimized unit of the R-SO_3-Cu^{II} is shown; the remaining atoms and hydrogen atoms in **1-SO_3H** are omitted for clarity.). C, black; O, red; N, blue; S, yellow; H, gray; Cu^{II}, cyan.

PXRD revealed that the pattern of **1-SO_3H** was not consistent with **1-SH-a**, but changed to match the PXRD pattern of **1-SH** (Figure 4a). The resulting formula of $[Zr_6(\mu_3\text{-}OH)_8(OH)_8][(Cu^{I}_{0.44}Cu^{II}_{0.56}(OH)_{0.56})_4(L_2)_4]_2{\cdot}3(C_4H_8O){\cdot}(C_3H_6O){\cdot}2H_2O$ (**1-SO_3H**) was defined from the combination of PXRD, XPS, ^{1}H NMR, IR spectra, ICP-AES, EA and TGA along with the reasonable deduction of oxidation states based on L_1^{2-} and Cu(I) (Section VI†).[32] Although scanning electron microscopy (SEM) confirmed that the shapes of single crystals of **1-SO_3H** remain, the structure of **1-SO_3H** could not be determined by SCXRD due to the cracking of crystals (Figures S3 and S9), leading to very weak diffraction. Thus, we modeled **1-SO_3H** using the framework of **1-SH** as a constraint and geometrically optimized the models using periodic density functional theory (DFT) calculations using the CP2K code (Section VII †).[33] The newly formed sulfonate anions coordinate in a bidentate fashion to Cu(II), either in a bridging mode or in chelating and bridging modes to two Cu(II) ions. Cu(II) was then allowed to coordinate to N atom of pyridine unit, and further coordinated to one -OH terminal to form 4- or 5-coodinated species (Figure 4b). TGA shows that **1-SO_3H** is not thermally stable and the activated sample was achieved by the exchange with acetone and dried at room temperature under vacuum for 24 h (Figure S5). **1-SO_3H** exhibits CO_2 adsorption at 273 K with maximum capacity of 32.0 $cm^3\ g^{-1}$ (Figure S6).

Scheme 2. (a) Styrene oxide ring-opening reaction with isopropanol, (b) conversion and (c) regioselectivity of A catalyzed by 1-SH-a and 1-SO_3H.

Compared with ideal 12-connected Zr-MOFs, such as UiO-type series,[34] **1-SH-a** and **1-SO_3H** with lower connectivity (8-connected) can be seen with "inherent defects", and the terminal hydroxide groups (Zr-OH) can be considered as catalytic Brønsted acid sites.[35-39] To test the catalytic activities of **1-SH-a** and **1-SO_3H**, ring-opening of styrene oxide with a monohydric alcohol (*i.e.* isopropanol) was selected as a model reaction. This reaction is hardly processed in the absence of catalyst, due to the poor nucleophilicity of alcohols.[40,41] As shown in Scheme 2a, the reaction was carried out at 55 °C with 1 mol% MOF catalyst. In accordance with the two possible sites of nucleophilic attack of isopropanol on styrene oxide, two products are possible: the primary alcohol (A) and the secondary alcohol (B). After 8 h, the reactions led to a >90% conversion of styrene oxide, and the final conversion can reach ~100% after 24 h for both catalysts (Scheme 2b and Table S2). PXRD indicated that the crystallinity of both MOFs remained intact after catalysis (Figure S4). Recycling tests with three consecutive runs were performed without any significant loss of their catalytic activities to indicate the catalysts can be reused (Table S2).

Figure 5. Plausible mechanisms for styrene oxide ring-opening reaction catalyzed by different catalytic sites.

Interestingly, for **1-SH-a** tested, both products A and B were achieved with ~71% of the regioselectivity towards primary alcohol (A), whereas **1-SO_3H** gave a regioselectivity of ~99% (Scheme 2c, Fig. S13-14 and Table S2). The regioselectivity of **1-SH-a** (71%) and **1-SO_3H** (99%) toward primary alcohol (A) was almost identical throughout the reaction course. This observation can be further rationalized by a first-order parallel reaction model (Section VIII †). From mechanistic point of view, generally, the ring-opening reaction of epoxides can proceed by either SN1 or SN2 mechanisms, depending on the nature of the catalyst and reaction conditions. Accordingly, plausible reaction mechanisms are proposed: (1) When styrene oxide undergoes in presence of an acidic catalyst, ring-opening occurs by an SN1 mechanism, and the more-substituted carbon is the site of attack, leading to product A. (2) Conversely, when initiating with a basic catalyst, the reaction takes place by a mechanism with substantial SN2 character, and the less-substituted carbon is the site of nucleophilic attack. As a result, product B predominates.[42] As shown in Figure 5, **1-SH-a** possesses $[Zr_6(\mu_3\text{-}OH)_8(OH)_8]^{8+}$ (Zr_6 nodes) and cuprous sulfur clusters (R-S-Cu^{I}), in which there is Zr_6 nodes-based Brønsted acid available to protonate the oxygen atom in styrene oxide to create a good leaving group, resulting in product A (I). This matched well with the product catalyzed by the previously reported benchmark Zr-MOFs.[40,41] For $R\text{-}S^-$, divalent organic sulfides are well-known strong Lewis bases and have stronger electron-donating ability. Thus, a deprotonated, negatively charged alkoxide is preferentially created. An alkoxide is a poor leaving group, making the ring unlikely to open without a "push" from the nucleophile, and the reaction is very likely to proceed by an SN2 mechanism (II). Clearly, this illuminates that both products A and B were observed when using Brønsted

acid sites and strong Lewis bases dual-functionalized **1-SH-a**. After postsynthetic oxidation, **1-SH-a** was completely accessible to form **1-SO_3H**, with retained Zr_6 nodes and newly formed R-SO_3-$Cu^{II}_{0.56}$-$OH_{0.56}$ units. Cu(II)-MOFs were found to be effective for the ring-opening reaction of styrene oxide with unsaturated coordinated Cu(II) sites as Lewis acids.[43-45] In this case, three types of plausible mechanisms could probably be adopted simultaneously and give an integrative contribution to the catalytic performance in **1-SO_3H**. Besides mechanism I, Lewis acidic Cu(II) binds to styrene oxide to produce an enhanced electrophilic nature of the carbon attached to the phenyl group through an acid – base interaction. Subsequently, the carbon with a partial positive charge is attacked by isopropanol to give product A (III). In addition, R-SO_3^- moieties might be protonated by inherent -OH from Zr-OH or Cu^{II}-OH in **1-SO_3H** and form strong Brønsted acidic R-SO_3H sites for alcoholysis of epoxides (IV).[46] Nevertheless, only product A is exclusively obtained within the above three proposed mechanisms, which is consistent with the experimental data observed in this work.

CONCLUSION

In conclusion, a water-stable heterometallic Zr-MOF with "primary" and "secondary" nodes has been reported, and the guest-dependent structural dynamic was studied by SCXRD. The presence of "primary" nodes in the framework plays a vital role in the improvement of structural stability. Subsequently, postsynthetic oxidation induced coordination site modification was successfully observed in "secondary" nodes. In addition, the catalytic behavior toward the styrene oxide ring-opening reaction after PSM was tuned, and plausible mechanisms were also unambiguously verified. The present work not only demonstrates a suitable MOF model for investigating the coordination site modification but also provides a potential prediction on the unique design of heterogeneous catalysts at the molecular level. Furthermore, postsynthetic oxidation of coordination site is expected to become a promising strategy for the introduction of multi-functionalities in MOFs for advanced applications.

ASSOCIATED CONTENT

Supporting Information.

The Supporting Information including synthesis of MOFs, PXRD, FT-IR, TGA, SEM, ^{1}H NMR, XPS, catalysis reaction, DFT calculation and crystal data is available free of charge on the ACS Publications website.

Crystallographic data for **1-SH** and **1-SH-a** (CIF)

AUTHOR INFORMATION

Corresponding Author

Yi Han – Key Laboratory of Eco-chemical Engineering, College of Chemistry and Molecular Engineering, Qingdao University of Science and Technology, Qingdao 266042, China; ocrid.org/0000-0003-0395-1111; Email: roberthan@yeah.net

Praveen K. Thallapally – Pacific Northwest National Laboratory, Richland, Washington 99352, United States; Email: praveen.thallapally@pnnl.gov

Author

Michael A. Sinnwell – Pacific Northwest National Laboratory, Richland, Washington 99352, United States

Robert G. Surbella III – Pacific Northwest National Laboratory, Richland, Washington 99352, United States

Wenjuan Xue – State Key Laboratory of Separation Membranes and Membrane Processes, Tianjin Polytechnic University, Tianjin 300387, China

Hongliang Huang – State Key Laboratory of Separation Membranes and Membrane Processes, Tianjin Polytechnic University, Tianjin 300387, China

Jian Zheng – Pacific Northwest National Laboratory, Richland, Washington 99352, United States

Bo Peng – Pacific Northwest National Laboratory, Richland, Washington 99352, United States

Gaurav Verma – Department of Chemistry, University of South Florida, Tampa, Florida 33620, United States

Yang Yang – Pacific Northwest National Laboratory, Richland, Washington 99352, United States

Lili Liu – Pacific Northwest National Laboratory, Richland, Washington 99352, United States

Shengqian Ma – Department of Chemistry, University of South Florida, Tampa, Florida 33620, United States

ACKNOWLEDGMENT

This work was supported by the U.S. DOE, Office of Science, Basic Energy Sciences, Division of Materials Sciences and Engineering, under Award KC020105-FWP12152. Department of Energy by BattellePNNL is a multiprogram national laboratory operated for the U.S. Memorial Institute under Contract DE-AC05-76RL01830. Y.H. acknowledges the support of the NSF of China (No. 21601102), the NSF of Shandong Province (No. ZR2016BQ34), the "International Postdoctoral Exchange Fellowship Program" (No. 20170035), and the Scientific and Technical Development Project of Qingdao (No.18-2-2-32-jch). RGS is grateful for the support of the Linus Pauling Distinguished Postdoctoral Fellowship program at PNNL.

REFERENCES

(1) Mehdi, A.; Reye, C.; Corriu, R. From molecular chemistry to hybrid nanomaterials. Design and functionalization. *Chem. Soc. Rev.* **2011**, *40*, 563–574.

(2) Brühwiler, D. Postsynthetic functionalization of mesoporous silica. *Nanoscale*. **2010**, *2*, 887–892.

(3) Cohen, S. M. Postsynthetic Methods for the Functionalization of Metal-Organic Frameworks. *Chem. Rev.* **2012**, *112*, 970–1000.

(4) Hendon, C. H.; Rieth, A. J.; Korzyński, M. D.; Dincă, M. Grand Challenges and Future Opportunities for Metal-Organic Frameworks. *ACS Cent. Sci.* **2017**, *3*, 554–563.

(5) Han, Y.; Li, J.-R.; Xie, Y.; Guo, G. *Chem. Soc. Rev.* Substitution reactions in metal–organic frameworks and metal–organic polyhedra. **2014**, *43*, 5952–5981.

(6) Wang, H.; Meng, W. Wu, J.; Ding, J.; Hou, H.; Fan, Y. Crystalline central-metal transformation in metal-organic frameworks. *Coord. Chem. Rev.* **2016**, *307*, 130–146.

(7) Wang, Z.; Cohen, S. M. *Chem. Soc. Rev.* Postsynthetic modification of metal–organic frameworks. **2009**, *38*, 1315–1329.

(8) Falkowski, J. M.; Wang, C.; Liu, S.; Lin, W. Actuation of asymmetric cyclopropanation catalysts: reversible single-crystal to single-crystal reduction of metal-organic frameworks. *Angew. Chem. Int. Ed.* 2011, 50, 8674–8678.

(9) McTernan, C. T.; Ronson, T. K.; Nitschke, J. R. Post-assembly Modification of Phosphine Cages Controls Host-Guest Behavior. *J. Am. Chem. Soc.* **2019**, *141*, 6837–6842.

(10) Liu, T.-F.; Zou, L.; Feng, D.; Chen, Y.-P.; Fordham, S.; Wang, X.; Liu, Y.; Zhou, H.-C. Stepwise synthesis of robust metal-organic frameworks via postsynthetic metathesis and oxidation of metal nodes in a single-crystal to single-crystal transformation. *J. Am. Chem. Soc.* **2014**, *136*, 7813–7816.

(11) Burnett, B. J.; Barron, P. M.; Hu, C.; Choe, W. Stepwise synthesis of metal-organic frameworks: replacement of structural organic linkers. *J. Am. Chem. Soc.* **2011**, *133*, 9984 – 9987.

(12) Li, T.; Kozlowski, M. T.; Doud, E. A.; Blakely, M. N.; Rosi, N. L. Stepwise ligand exchange for the preparation of a family of mesoporous MOFs. *J. Am. Chem. Soc.* **2013**, *135*, 11688 – 11691.

(13) Taddei, M.; Wakeham, R, J.; Koutsianos, A.; Andreoli E.; Barron, A. R. Post-Synthetic Ligand Exchange in Zirconium-Based Metal-Organic Frameworks: Beware of The Defects! *Angew. Chem. Int. Ed.* **2018**, *57*, 11706–11710.

(14) Karagiaridi, O.; Bury, W.; Mondloch, J. E.; Hupp J. T.; Farha, O. K. Solvent-assisted linker exchange: an alternative to the de novo synthesis of unattainable metal-organic frameworks. *Angew. Chem. Int. Ed.* **2014**, *53*, 4530–4540.

(15) Shao, Z.; Huang, C.; Dang, J.; Wu, Q.; Liu, Y.; Ding, J.; Hou, H. Modulation of Magnetic Behavior and Hg^{2+} Removal by Solvent-Assisted Linker Exchange Based on a Water-Stable 3D MOF. *Chem. Mater.* **2018**, *30*, 7979–7987.

(16) Song, Y.-F.; Cronin, L. Postsynthetic Covalent Modification of Metal–Organic Framework (MOF) Materials. *Angew. Chem. Int. Ed.* **2008**, *47*, 4635–4637.

(17) Sun, F.; Yin, Z.; Wang, Q.-Q.; Sun, D.; Zeng M.-H.; Kurmoo, M. Tandem Postsynthetic Modification of a Metal – Organic Framework by Thermal Elimination and Subsequent Bromination: Effects on Absorption Properties and Photoluminescence. *Angew. Chem. Int. Ed.* **2013**, *52*, 4538–4543.

(18) Vermeulen, N. Karagiaridi, A. O.; Sarjeant, A. A.; Stern, C. L.; Hupp, J. T.; Farha, O. K.; Stoddart, J. F. Aromatizing Olefin Metathesis by Ligand Isolation inside a Metal – Organic Framework. *J. Am. Chem. Soc.* **2013**, *135*, 14916–14919.

(19) Qin, J.-S.; Yuan, S.; Zhang, L.; Li, B.; Du, D.-Y.; Huang, N.; Guan, W.; Drake, H. F.; Pang, J.; Lan, Y.-Q.; Alsalme, A.; Zhou, H.-C. Creating Well-Defined Hexabenzocoronene in Zirconium Metal-Organic Framework by Postsynthetic Annulation. *J. Am. Chem. Soc.* **2019**, *141*, 2054–2060.

(20) Jin, R.; Zeng, C.; Zhou, M.; Chen, Y. Atomically Precise Colloidal Metal Nanoclusters and Nanoparticles: Fundamentals and Opportunities. *Chem. Rev.* **2016**, *116*, 10346–10413.

(21) Lobana, T. S.; Kinoshita, I.; Kimura, K.; Nishioka, T.; Shiomi, D.; Isobe, K. Pyridine-2-sulfonates as Versatile Ligands for the Synthesis of Novel Coordinative and Hydrogen-Bonded Supramolecules. *Eur. J. Inorg. Chem.* **2004**, *2*, 356–367.

(22) Adams, L.; Oki, A.; Grady, T.; McWhinney, H.; Luo, Z. Preparation and characterization of sulfonic acid-functionalized single-walled carbon nanotubes. *Physica E Low Dimens Syst Nanostruct.* **2009**, *41*, 723–728.

(23) Adam, W.; Grimm, G. N.; Marquardt, S.; Saha-Möller, C. R. Are Pyridinethiones Reliable Photochemical Oxyl-Radical Sources for Photobiological Studies? The Importance of Secondary Photolysis Products in the Guanine Oxidation of 2‘-Deoxyguanosine and Cell-Free DNA. *J. Am. Chem. Soc.* **1999**, *121*, 1179–1185.

(24) Han, Y.; Zheng, H.; Liu, K.; Wang, H.; Huang, H.; Xie, L.-H.; Wang, L.; Li, J.-R. In-Situ Ligand Formation-Driven Preparation of a Heterometallic Metal – Organic Framework for Highly Selective Separation of Light Hydrocarbons and Efficient Mercury Adsorption. *ACS Appl. Mater. Interfaces.* **2016**, *8*, 23331–23337.

(25) Zhang, Y.; Zhang, X.; Lyu, J.; Otake, K.; Wang, X.; Redfern, L. R.; Malliakas, C. D.; Li, Z.; Islamoglu, T.; Wang, B.; Farha, O. K. A Flexible Metal-Organic Framework with 4-Connected Zr6 Nodes. *J. Am. Chem. Soc.* **2018**, *140*, 11179–11183.

(26) Kim, H.; Kim, D.; Moon, D.; Choi, Y. N.; Baek, S. B.; Lah, M. S. Symmetry-guided syntheses of mixed-linker Zr metal-organic frameworks with precise linker locations. *Chem. Sci.* **2019**, *10*, 5801–5806.

(27) Zhao, X.; Shimazu, M. S.; Chen, X.; Bu, X.; Feng, P. Homo-Helical Rod Packing as a Path Toward the Highest Density of Guest-Binding Metal Sites in Metal–Organic Frameworks. *Angew. Chem. Int. Ed.* **2018**, *57*, 1–5.

(28) Bai, Y.; Dou, Y.; Xie, L.-H.; Rutledge, W.; Li J.-R.; Zhou, H.-C. Zr-based metal-organic frameworks: design, synthesis, structure, and applications. *Chem. Soc. Rev.* **2016**, *45*, 2327–2367.

(29) Colombo, V.; Galli, S.; Choi, H. J.; Han, G. D.; Maspero, A.; Palmisano, G.; Masciocchic, N.; Long. J. R. High thermal and chemical stability in pyrazolate-bridged metal–organic frameworks with exposed metal sites. *Chem. Sci.* **2011**, *2*, 1311–1319.

(30) Saikia, M.; Saikia, L. Sulfonic acid-functionalized MIL-101(Cr) as a highly efficient heterogeneous catalyst for one-pot synthesis of 2-

amino-4H-chromenes in aqueous medium. *RSC Adv.* **2016**, *6*, 15846–15853.

(31) Tu, B.; Pang,Q.; Xu, H.; Li, X.; Wang, Y.; Ma, Z.; Weng, L.; Li, Q. Reversible Redox Activity in Multicomponent Metal–Organic Frameworks Constructed from Trinuclear Copper Pyrazolate Building Blocks. *J. Am. Chem. Soc.* **2017**, *139*, 7998–8007.

(32) Liao, P.-Q.; Chen, H.; Zhou, D.-D.; Liu, S.-Y.; He, C.-T.; Rui, Z.; Ji, H.; Zhang, J.-P.; Chen, X.-M. Monodentate hydroxide as a super strong yet reversible active site for CO2capture from high-humidity flue gas. *Energy Environ. Sci.* **2015**, *8*, 1011–1016.

(33) Accelrys, Inc., Materials Studio, 4.3V, Accelrys, Inc., San Diego, CA, 2008.

(34) Cavka, J. H.; Jakobsen, S.; Olsbye, U.; Guillou, N.; Lamberti, C.; Bordiga, S.; Lillerud, K. P. A new zirconium inorganic building brick forming metal organic frameworks with exceptional stability. *J. Am. Chem. Soc.* **2008**, *130*, 13850–13851.

(35) Katz, M. J.; Mondloch, J. E.; Totten, R. K.; Park, J. K.; Nguyen, S. T.; Farha O. K.; Hupp, J. T. Simple and compelling biomimetic metal-organic framework catalyst for the degradation of nerve agent simulants. *Angew. Chem., Int. Ed.* **2014**, *53*, 497–501.

(36) Corma, A.; García, H.; Llabrés i Xamena, F. X. Engineering metal organic frameworks for heterogeneous catalysis. *Chem. Rev.* **2010**, *110*, 4606–4655.

(37) Yoon, M.; Srirambalaji, R.; Kim, K. Homochiral metal-organic frameworks for asymmetric heterogeneous catalysis. *Chem. Rev.* **2012**, *112*, 1196–1231.

(38) Moon, S.-Y.; Liu, Y.; Hupp J. T.; Farha, O. K. Instantaneous hydrolysis of nerve-agent simulants with a six-connected zirconium-based metal-organic framework. *Angew. Chem., Int. Ed.* **2015**, *54*, 6795–6799.

(39) Ravon, U.; Savonnet, M.; Aguado, S.; Domine, M. E.; Janneau, E.; Farrusseng, D. Engineering of coordination polymers for shape selective alkylation of large aromatics and the role of defects. Microporous Mesoporous Mater. **2010**, *129*, 319–329.

(40) Liu, Y.; Klet, R. C.; Hupp, J. T.; Farha, O. K. Probing the correlations between the defects in metal – organic frameworks and their catalytic activity by an epoxide ring-opening reaction. *Chem. Commun.* **2016**, *52*, 7806–7809.

(41) Tan, Y.-X.; Yang, X.; Li, B.-B.; Yuan, D. Rational design of a flu-type heterometallic cluster-based Zr-MOF. *Chem. Commun.* **2016**, *52*, 13671–13674.

(42) McMurry, J. Organic Chemistry 9th edition, Chapter 18.6: Reactions of Epoxides - Ring-opening. **2016**, *Cengage Learning*, Raleigh.

(43) Dhakshinamoorthy, A.; Alvaro, M.; Garcia, H. Metal – Organic Frameworks as Efficient Heterogeneous Catalysts for the Regioselective Ring Opening of Epoxides. *Chem. Eur. J.* **2010**, *16*, 8530–8536.

(44) Jiang, D.; Urakawa, A.; Yulikov, M.; Mallat, T.; Jeschke, G.; Baiker, A. Size selectivity of a copper metal-organic framework and origin of catalytic activity in epoxide alcoholysis. *Chem. Eur. J.* **2009**, *15*, 12255–12262.

(45) Jiang, D.; Mallat, T.; Krumeich, F.; Baiker, A. Copper-based metal-organic framework for the facile ring-opening of epoxides. *J. Catal.* **2008**, *257*, 390–395.

(46) Zhou, Y.-X.; Chen, Y.-Z.; Hu, Y.; Huang. G.; Yu, S.-H.; Jiang, H.-L. MIL-101-SO_3H: a highly efficient Brønsted acid catalyst for heterogeneous alcoholysis of epoxides under ambient conditions. *Chem. Eur. J.* **2014**, *20*, 14976–14980.

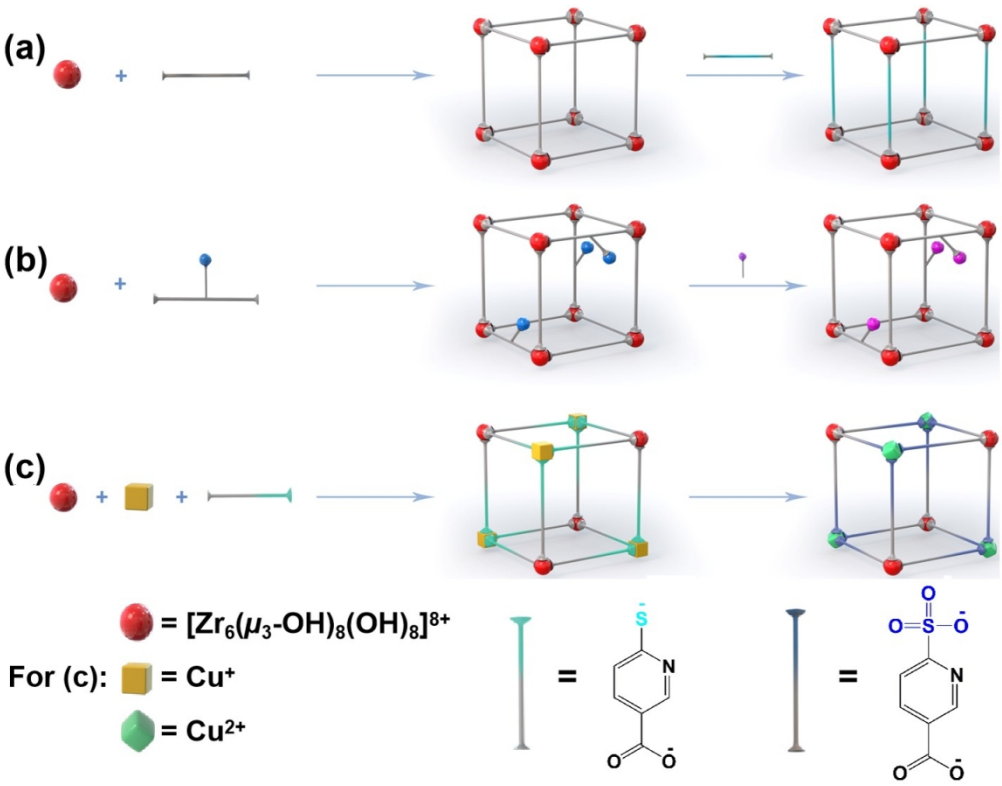

Scheme 1

241x188mm (150 x 150 DPI)

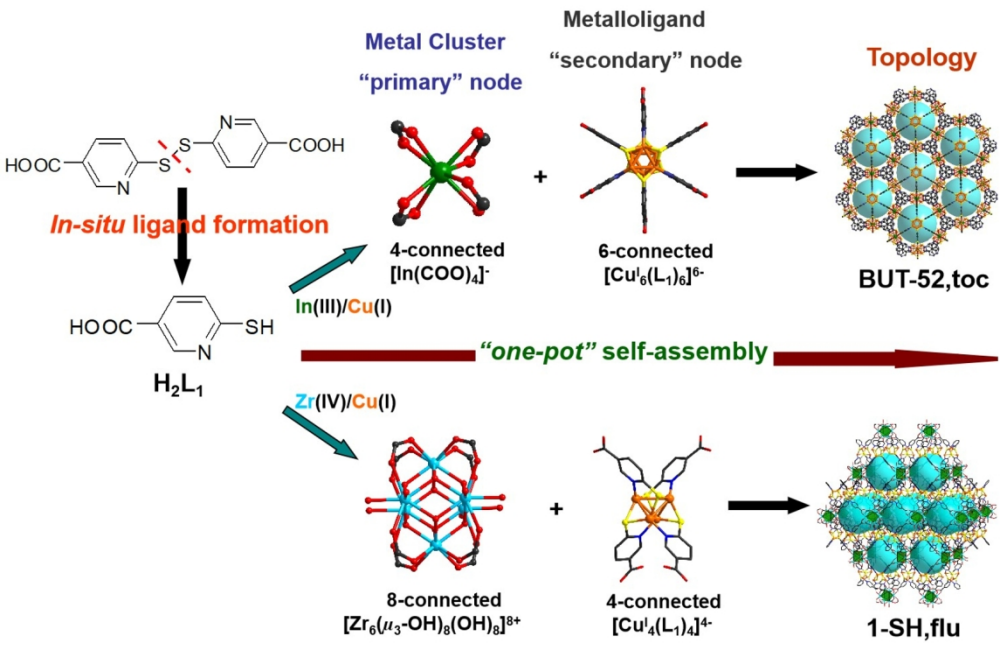

Figure 1

289x190mm (150 x 150 DPI)

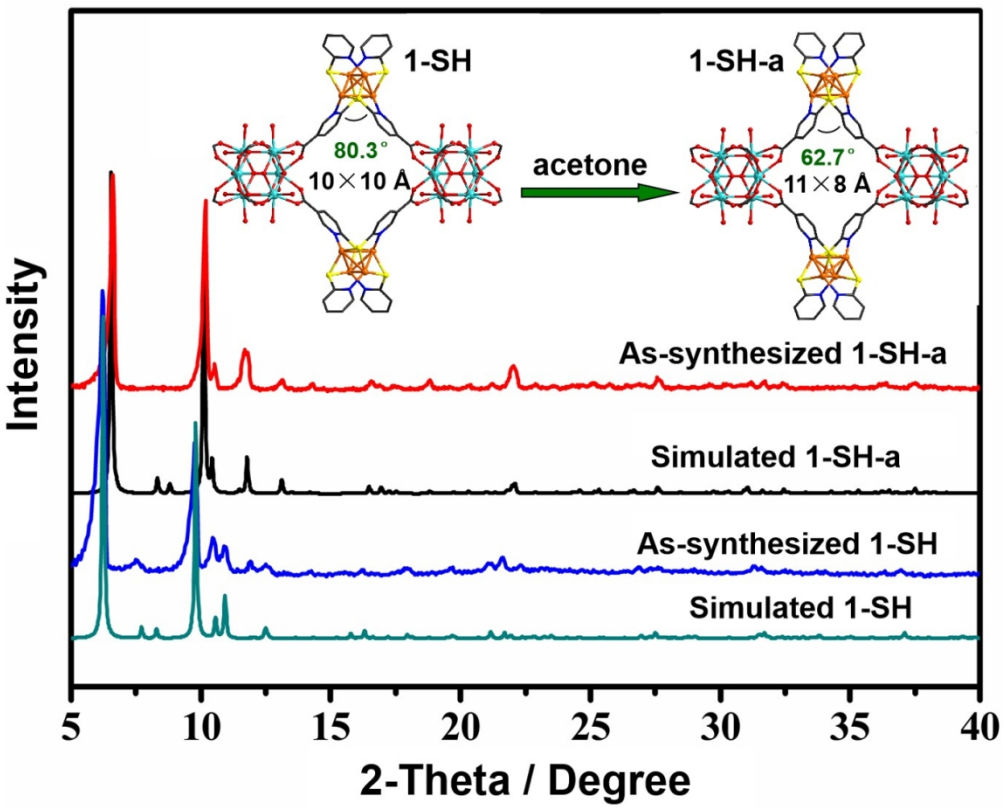

Figure 2

234x190mm (150 x 150 DPI)

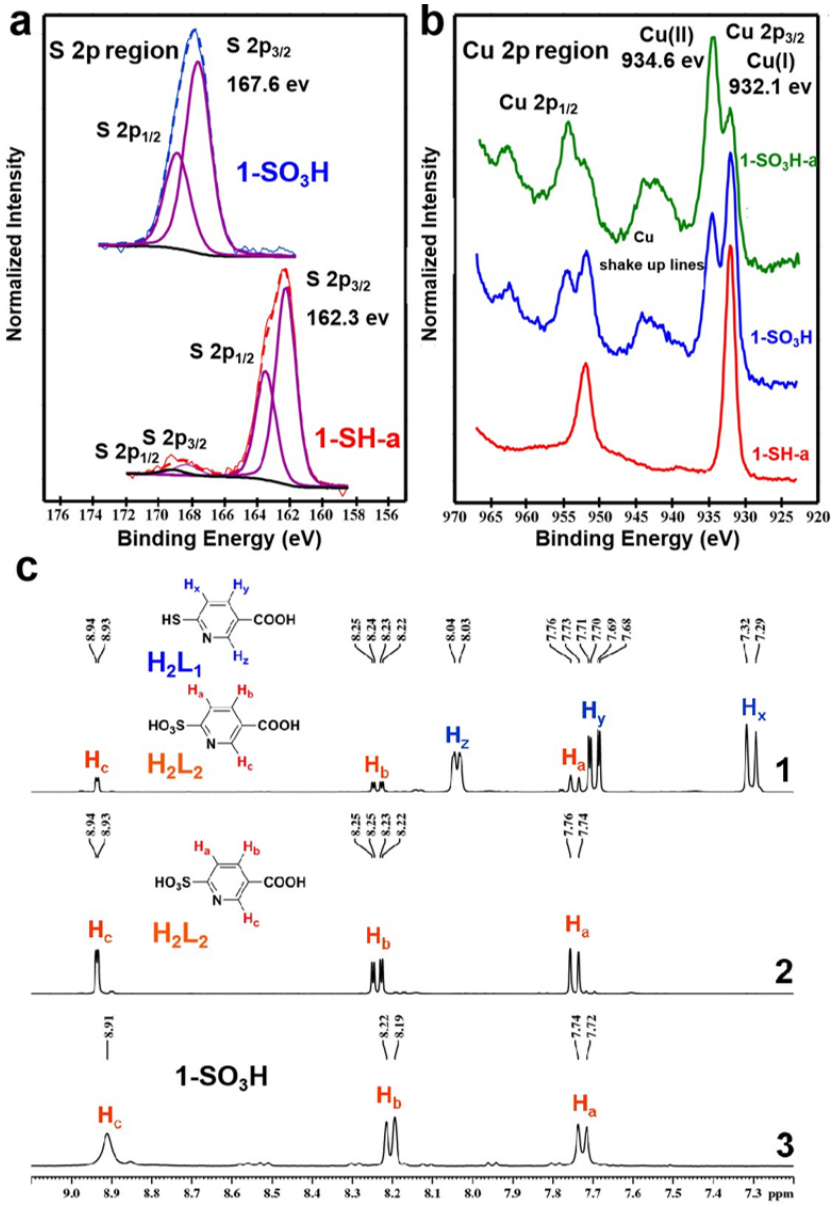

Figure 3

131x190mm (150 x 150 DPI)

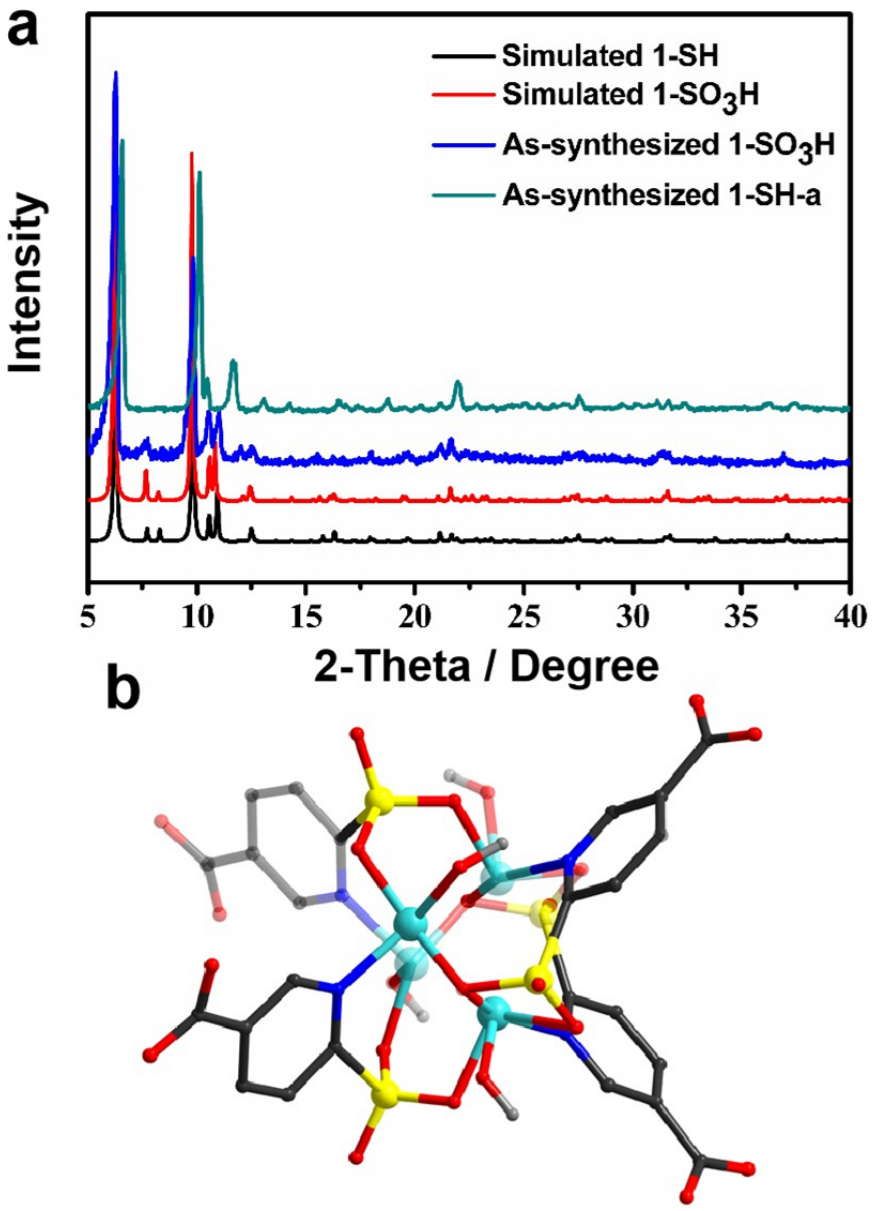

Figure 4

136x189mm (150 x 150 DPI)

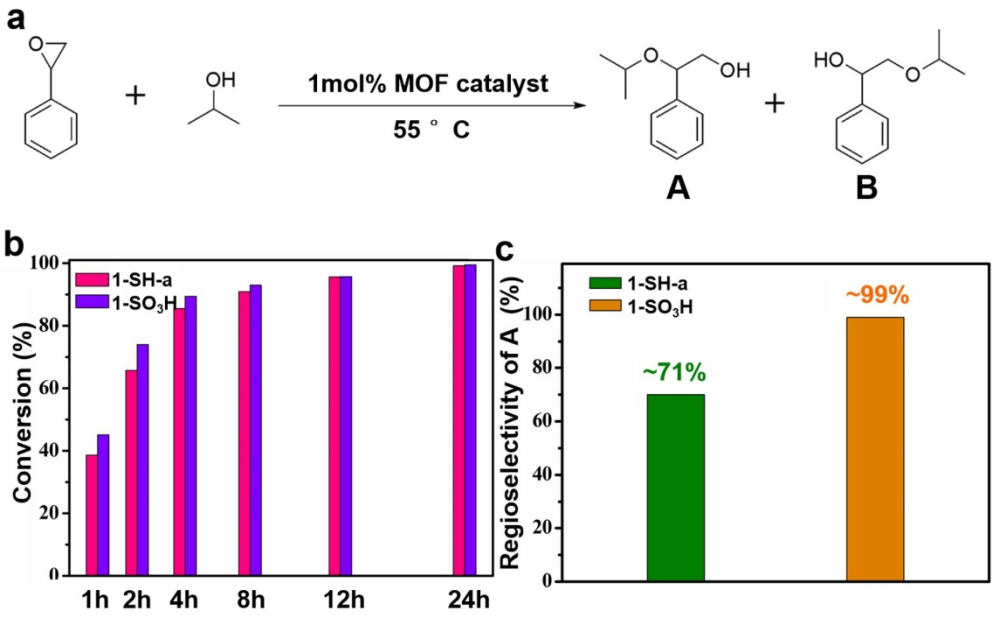

Scheme 2

316x190mm (150 x 150 DPI)

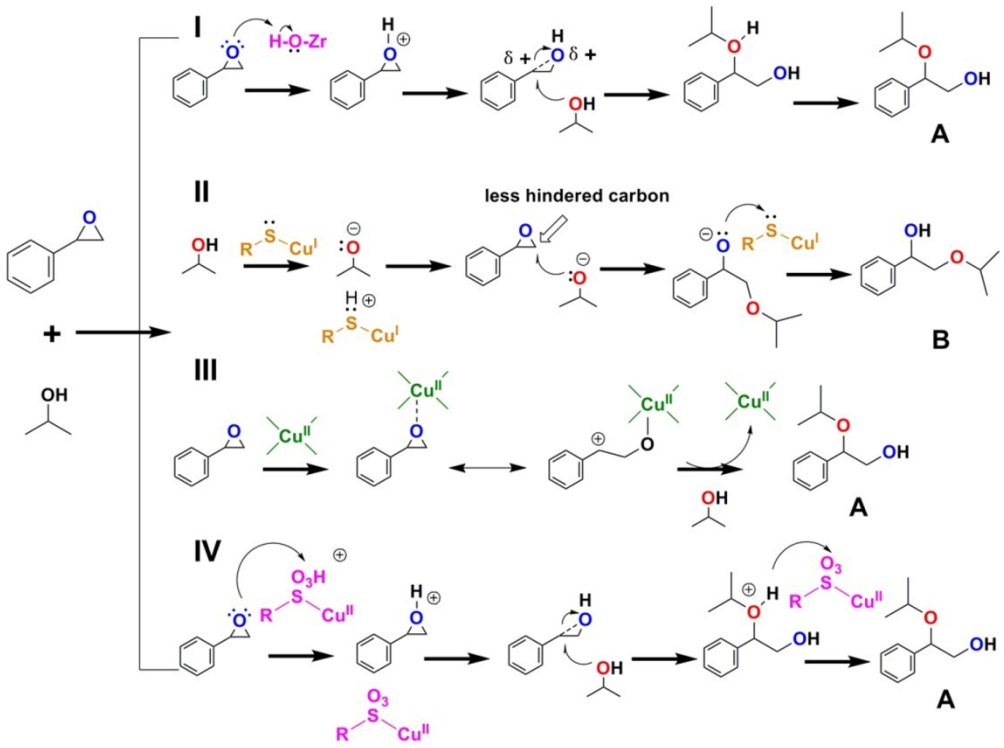

Figure 5

256x190mm (150 x 150 DPI)

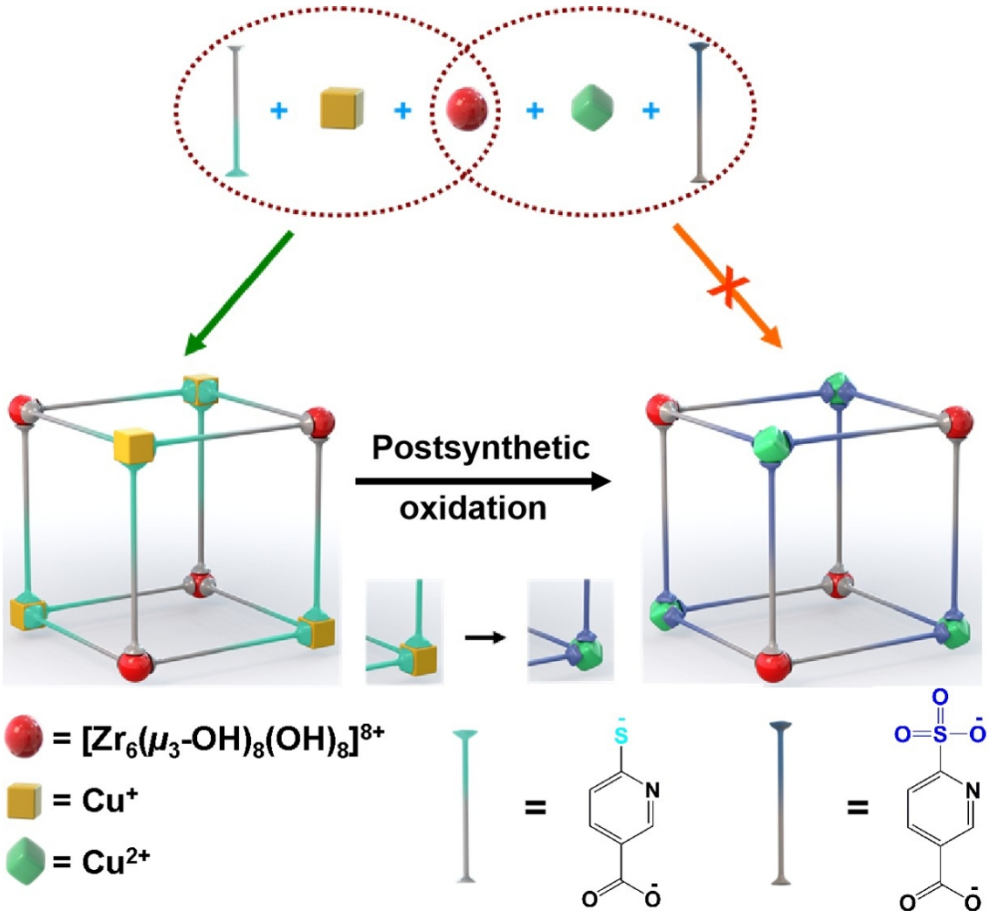

ToC graphic for this manuscript

210x189mm (150 x 150 DPI)